IET Cyber-Physical Systems: Theory & Applications

Research Article

IET Journals
The Institution of Engineering and Technology

Flocking-based adaptive granular control strategy for autonomous microgrids in emergency situations

ISSN 2398-3396
Received on 19th May 2018
Revised 15th August 2018
Accepted on 17th September 2018
E-First on 14th January 2019
doi: 10.1049/iet-cps.2018.5019
www.ietdl.org

Moein Sabounchi[1] ✉, *Jin Wei*[1], *Dongchan Lee*[1], *Deepa Kundur*[1]

[1]*Department of Electrical and Computer Engineering, The University of Akron, Akron, Ohio, USA*

✉ *E-mail: ms370@zips.uakron.edu*

Abstract: In this study, the authors study the operation of autonomous microgrids (MGs) in emergency situations such as the presence of large physical disturbances or cyber attacks. Traditional approaches to enhance system-wide stability, such as automatic generation control, are insufficient for stabilising MGs in some emergency situations due to the correspondingly lower capacity of distributed energy resources. To address this challenge, in this study, they develop an adaptive flocking-based framework that provides control-based MG resilience. The contribution of the authors' work is three-fold. First, they effectively model the complex and dynamic dependencies amongst MG components by exploiting flocking theory. Second, they propose an adaptive granular control strategy based on the modelled dynamic dependencies. Third, they also explore the role of energy storage systems to facilitate distributed generations in achieving autonomous MG power balance in the presence of disruptions of different natures. Case studies demonstrate the effectiveness of the proposed strategy in stabilising MGs in response to physical disturbances and cyber attacks.

1 Introduction

The smart grid design mantra for evolution can be described, in part, as 'knowledge is power.' In smart grids, advanced measurement, two-way communication technologies, and computational intelligence are applied to the power grid [1]. This helps to provide an integrated cyber-physical operation that is more efficient, reliable and resilient through greater situational awareness [2].

A microgrid (MG) is a medium or low voltage network that consists of a cluster of loads and exhibits a high depth of distributed energy resource (DER) penetration. Typical DERs include the dispatchable distributed generators (DDGs) and energy storage systems (ESSs). MG operation and control is based on information and communication technologies. Thus, the MG represents a *cyber-physical* building block for the smart grid that provides a convenient and scalable way to introduce DERs at the distribution level. The MG is interfaced to the main grid at a point of common coupling (PCC) and is able to operate in a grid-connected or an islanded mode. In order to ensure the efficient operation in both modes and during their transition, the control system for an MG is typically identified to have three levels: primary, secondary, and tertiary [3]. At the highest level, tertiary control sets the steady-state nominal points when an MG is operating in [4]. The secondary control compensates for the voltage and frequency deviations with respect to the steady-state set points by determining the appropriate set points for the primary control [5]. Dynamic balancing is defined as a function at the secondary level that is responsible for matching generation and load while satisfying operational constraints of the MG. The primary control ensures that the system variables track their set points. In this paper, the authors focus on the challenging problem of enhancing the operational resilience of MG systems in islanded mode. As such, the authors are concerned with mid to long-term survivability of the MG and study issues of secondary power balancing control, which represents a rich and largely underdeveloped field of study.

Generally speaking, the automatic generation and voltage control (AGC/AVC) is essential for realising the regulation and control of the active and reactive power in both large-scale main grids and the MGs especially in emergency situations. As stated in [6], in large-scale power grids AGC/AVC mainly focuses on controlling primary power plant components such as excitation and prime mover. The critical settings for optimising AGC/AVC include inertia constant, governor time constant, turbine time constant and reheat time lag. However, due to the high penetration of the DERs that have inherent lower-inertia feature, there is a big challenge to apply the AGC/AVC techniques widely used in large-scale power grids to the MGs, especially to the ones in an islanded mode [7]. To address this challenge, different control mechanisms have been developed for the maintenance and operation of MGs. In [8], the authors proposed voltage source inverter (VSI) control-based conventional approaches to dynamically regulate the power output of DERs to achieve power balance in autonomous MGs after physical disturbance or cyber attacks. However, the effectiveness of these approaches is reduced for MGs with high non-synchronous generator integration. Furthermore, in the situations with the severe disturbances, such as the ones considered in this paper, the performance of VSI control-based approaches can be restricted by the limited power output capacity or energy capacity of the relevant MG components. To tackle this challenge, various secondary control strategies have been developed to coordinate the DERs and the controllable loads (CLs). In [5] a potential-function-based control strategy was proposed for secondary voltage control that exhibits efficient MG management with low computational complexity. In [9], the authors addressed secondary voltage control via a Lyapunov-based adaptive distributed control strategy that makes use of neural networks independent of DDG parameters. The proposed technique allows the independent control on the DDG parameters while being robust to a single point of failure. Additionally, a voltage control mechanism was proposed in [10] by applying an adaptive sliding mode theory, and a frequency regulation method was developed in [11] by designing a frequency feedback loop with PI control. Furthermore, Lou *et al.* in [12] developed a decentralised secondary voltage and frequency control in islanded MGs based on the state estimation principle and cooperative strategy. Xu *et al.* [13] propose a novel approach for MG secondary control based on a finite-time secondary frequency control algorithm which eliminates frequency deviation and provides an efficient active power sharing.

In this paper, we propose a flocking-based adaptive granular control strategy for secondary MG control in emergency situations. Our work consists of three main stages. First, we exploit the

flocking theory to model the complex and dynamic interaction amongst different MG components. Second, we design a set of models for characterising the MG's generation and demand cumulative signals. Third, we develop an adaptive control mechanism and reference-following in the system. Since the operation of these three stages is co-dependent and deployed in various layers of the system, the consequent model will be granular. In this granular model, the larger granulation encapsulates the reference model and its structure and the smaller one consists of the flocking model and reference following mechanism. Additionally, our control system as a whole is considered as a model-reference adaptive granular control strategy combined with flocking algorithm that is proposed for the secondary control of MGs to achieve AGC/AVC and stabilise frequency and voltage. The authors would like to claim that there are various control strategies for MG operation by considering different objectives such as minimising the power loss or maximising the income. In this paper, we focus on developing a resilient control strategy in the context of disaster conditions. As suggested in [14], restoring critical loads and power balance is the goal with the first priority in face of disasters and emergencies to avoid the potential cascading failures. Furthermore, in order to ensure the long-term sustainability of the operation, the balance of power in the MG must be met before the capability of frequency and voltage regulating generators reach its limit. Therefore, the authors believe that it is reasonable to focus on the secondary control to achieve power balance in the limited time. We explore the role of DERs in improving the resilience of autonomous MG systems. Specifically, the authors focus on how ESSs can be leveraged to enhance the reliability of DDGs through our proposed control strategy which is of utmost importance to the authors.

Furthermore, considering the high vulnerability of MGs to potential cyber attacks [15], in the simulation section, we evaluate the performance of our proposed control mechanism in the presence of cyber attacks. Various researches have been developed to study the cyber attacks against the confidentiality, integrity, and availability of power systems. For the attacks against availability, the authors in [16] studied the Denial of Service (DoS) attacks in autonomous MGs and proposed a controlling method by incorporating ESS systems as decentralised asynchronous generators to mitigate the impact of DoS attacks. The attacks against the confidentiality, such as eavesdropping, were studied in [17]. The work in [17–21] proposed a different mechanism for addressing the false data injection (FDI) attacks against integrity. The authors in [17] proposed a feedback linearisation technique and designed a control algorithm to conquer the transient abnormalities and disturbances caused by FDI attacks. Rana *et al.* in [18] proposed an algorithm to mitigate FDI attacks on power grids by using recursive systematic conventional code and Kalman filter. The authors of [20] investigated the impacts of the FDI attacks on the phasor measurement unit devices from the perspectives of AC-state and hybrid-state estimation, respectively. In the case of the hybrid estimator, the bus voltages and the branch currents were measured. The authors used an iterative algorithm to find the best estimate of the power system. A threshold of noise was then introduced to find and distinguish the faulty data from those affected by Gaussian noise. Data-driven detection methods on FDI attacks were proposed in [19, 21]. Wang *et al.* developed the methods by using margin setting algorithm and He *et al.* proposed the method by exploiting deep learning techniques. In this paper, we focus on evaluating the resilience of our proposed control algorithm against unexpected emergencies such as power imbalances and FDI attacks.

The next section introduces the specific focus of MG control for power balance. Section 3 presents the proposed flocking-based adaptive granular control strategy. Section 4 details the MG test system employed. Simulation results are presented in Section 5 followed by conclusions in Section 6.

2 Problem setting

In this work, the autonomous MG in an emergency situation is characterised as a cyber-physical system.

2.1 Architecture

The proposed cyber-physical system incorporates agents to represent the units of the system. Considering that in an emergency situation, the objective of timelessness of recovering the system has much higher priority than the objective of reducing computational complexity and communication cost, in this work, we assume that there exists an all-to-all communication network in the autonomous MG in which all MG units are connected to each other via communication links. A good practical example of such a system can be seen in *ABB Solutions* islanded MG development suites [22]. Additionally, the authors believe that it is feasible in a small MG, such as the one we focus on, to have that type of communication network as there are no scalability issues. Furthermore, we also assume that the MG units have the following main characteristics:

i. *Autonomous*: the units are partially independent and self-aware, which means that they share partial data on their status with the other MG units.
ii. *Social*: the units can communicate and coordinate with other units to achieve their objectives via the communication system.

2.2 Cyber-physical adaptive paradigm for autonomous MG modelling

According to different functions in the application of stability maintenance, various MG components are modelled by using the following four units:

i. *ESS unit* that is able to inject and absorb power from MGs and responds to changes in the environment quickly.
ii. *DDG unit* that is able to inject power into MGs and responds to the changes of the environment slower compared with ESS agent.
iii. *CL unit* whose power consumption can be adjusted.
iv. *Uncontrollable unit* whose power consumption or generation cannot be controlled.

For example, battery and flywheel energy storage are both modelled as ESS units, diesel generators and combined heat, power are both modelled as DDG unit, and wind turbine (WT) and, gas and uncontrollable loads are all, modelled as uncontrollable units. The authors would like to clarify that in this paper RES refers to the renewable energy source generation rather than the integration of RES generation together with energy storage. By considering the fact that renewable energy generation is highly intermittent in nature, RESs (WT) are modelled as uncontrollable units [23]. In our strategy, the uncontrollable units only communicate with their associated ESS units. Furthermore, all of the ESS, DDG and CL units have the capability of sensing the local environment, such as the stability of local frequency and voltage and carrying out the corresponding control actions. Therefore, all these three units are controllable.

As illustrated in Fig. 1, each controllable unit consists of two main interdependent control algorithms: flocking algorithm and model-reference adaptive control system (MRAS). The parameters of the reference model in the adaptive control section are derived based on the flocking model larger scale model. Afterwards, the controlling signal from the adaptive block controls the system which will, in turn, lead to update in the status of the system. It should be noted that the timescale of the flocking algorithm is much slower than the adaptive one and this allows us to use a model reference algorithm. For example, each ESS unit informs the other controllable units about its stored energy, instant power output, and the total power output of the local uncontrollable units. The DDG and CL units send the information on their power outputs and power demands, respectively. Using the information received via the all-to-all communication, each controllable unit adjusts the set point according to the flocking-based control scheme in a larger granulation and realise the final control based on the model-reference adaptive control system within a smaller granulation which is detailed in Section 3.2.4.

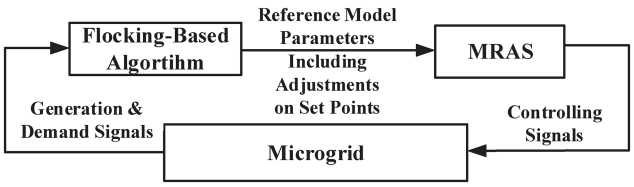

Fig. 1 *Interaction between different controllable units*

Table 1 Units' identifiers

Unit	Identifier (x)
storage system	b
generation unit	g
load	l

The authors assert that the formulation succinctly describes the complex interactions and coupled dependencies amongst the dynamic units of the MG. The proposed work focuses on designing the coordination between the individual portions of MGs under conditions of significant physical fault or cyber attack. In the scenarios, which this paper addresses, ESS units respond (within a short-time scale of milliseconds) to inject/absorb power to aid in system re-stabilisation. Concurrently, at a longer time scale, the set points of the DDG units' power outputs are updated and power demand of CL units is adjusted if necessary. Given the limited energy capacity of the ESS units, they respond to the grid for a narrow duration of time eventually bringing its power output to zero once a power balance of the overall system is achieved. The following paragraphs present how a flocking-based dynamic systems paradigm provides an elegant cyber-physical adaptive framework from which, we model the cooperation needed amongst the ESS, DDG and CL units under heavy disturbance conditions.

3 Granular algorithm with flocking-based adaptive control

This paper considers a general MG that consists of k ESS units, m DDG units, n CL units, as well as non-controllable units. The cyber-physical dynamics of each unit is described using state variables (x, v) and control u with appropriate subscript indices. Moreover, this paper denotes the stored energy and power output of the ith ESS unit with $E_{B,i}$ and $P_{B,i}$, respectively, the power output of the ith DDG unit and the ith CL unit with $P_{G,i}$ and $P_{L,i}$, respectively, and the power differential at two consecutive monitoring time steps for DDG and CL units as $\Delta P_{G,i}$ and $\Delta P_{L,i}$. Where applicable, the corresponding set points of the model for the variables above are denoted with an asterisk to give $E^*_{B,i}$, $P^*_{G,i}$ and $P^*_{L,i}$.

3.1 Flocking formation control

The mathematical modelling of bird-like flocking behaviour began with Reynolds' seminal work [24] in which he proposed three heuristic rules that led to the synthesis of the first computer animation of flocking: (i) *flock centring*, (ii) collision avoidance, and (iii) *velocity matching*. Based on these three rules, a distributed flock formation control framework was later proposed by Olfati-Saber in [25] with the following dynamics:

$$\dot{\boldsymbol{q}} = \boldsymbol{p}, \quad \dot{\boldsymbol{p}} = \tilde{\boldsymbol{u}} \tag{1}$$

where $\boldsymbol{q}$ and $\boldsymbol{p}$ are the position and velocity vectors of the flockmates, respectively, and $\tilde{\boldsymbol{u}}$ is the following control strategy:

$$\tilde{\boldsymbol{u}} = -\nabla V(\boldsymbol{q}) - \boldsymbol{L}\cdot\boldsymbol{p} + F(\boldsymbol{p}, \boldsymbol{q}, \boldsymbol{p}_r, \boldsymbol{q}_r) \tag{2}$$

The first term of (2) represents the gradient of a potential energy function $V(\boldsymbol{q})$ that characterises flocking system objectives and constraints. The second represents a velocity consensus protocol where $\boldsymbol{L}$ is the Laplacian matrix associated with an associated flock communication graph. The third component models navigational feedback designed to ensure that the unit states converge to desired values $(\boldsymbol{p}_r, \boldsymbol{q}_r)$.

The next section presents the modelling of ESS, DDG and CL units in the MG and applies flocking theory to identify a distributed control paradigm for power balance under disruption.

3.2 Proposed adaptive granular control strategy

To enable the use of the adaptive control strategy, the proposed strategy employs fixed-order model-fitting techniques to describe the dynamic behaviour of each type of agents [26–28]. Given the time scale of the secondary control, that is the focus of this paper, a second-order transfer function for each agent is adopted. More specifically, the proposed strategy employs a fixed-order transfer function for each unit whose parameters must be identified. In other words, we assume the dynamics of the model with a second-order estimate of them. The parameters of these estimates are subject to volatilities and during the function of the system they may change in one or another direction, henceforth we are forced to use a pre-determined model for the performance of the parameters of the system. This leads us to the adaptive section of control portfolio. Due to this, we proposed a MRAS method to maximise the efficiency and minimise the error ratio of the unit parameters to their ideal performance. The detailed description of this model will be explained in Section 3.2.4. The dynamics and models incorporated to model different types of grid components are presented below.

3.2.1 Grid components models: As mentioned earlier, from the prospective of control, the MG units, can generally be categorised into three main groups: ESSs, DDG Units, and CL Units. The general model for each of these units can be described as the following equation:

$$\begin{cases} E_{x,i}(s) = G_{x,i}(s)E^*_{x,i}(s), \\ P_{x,i}(s) = -sE_{x,i}(s) \end{cases} \tag{3}$$

where x represents the identifying parameter of each type of unit and is specified in Table 1.

The models of the individual units based on these identifiers are detailed in the followings.

ESS unit: Although the proposed modelling framework can apply to different types of ESS units, this paper considers one specific ESS type, battery ESSs (BESSs), where $E_{B,i}(s)$ is the stored energy of the ith BESS, $P_{B,i}(s)$ is the output power of the ith BESS, $E^*_{B,i}(s) = u_{B,i}(s)$ represents the set point for the output energy of the ith BESS that is assigned to the value of the control signal in the proposed framework, $G_{B,i}(s)$ denotes the transfer function of the ith BESS and is given by

$$G_{B,i}(s) = \frac{k_{B,i}}{a_{B,i}s^2 + b_{B,i}s + 1} \tag{4}$$

where $k_{B,i}$, $a_{B,i}$, and $b_{B,i}$ are parameters that characterise the dynamics of the BESS by considering the time scale of the proposed control strategy. Furthermore, the dynamics of BESS incorporate rate of charge by appropriately setting the parameters.

Based on (3), a dynamic systems representation of the BESS is developed. Variable substitutions $x_{B,i}(t) = E_{B,i}(t)$ and $v_{B,i}(t) = P_{B,i}(t)$ are made to achieve the following state-space representation for BESSs:

$$\begin{cases} \dot{x}_{B,i}(t) = -v_{B,i}(t), \\ \dot{v}_{B,i}(t) = -\dfrac{b_{B,i}}{a_{B,i}} v_{B,i}(t) + \dfrac{1}{a_{B,i}} x_{B,i}(t) - \dfrac{k_{B,i}}{a_{B,i}} u_{B,i}(t) \end{cases} \tag{5}$$

To model the limited energy capacity $E_{B,i}^{\max}$ and bounded maximum output power $P_{B,i}^{\max}$ of the BESS in both charging and discharging modes, the following constraints on the state of BESS are introduced:

$$\begin{cases} 0 \le x_{B,i}(t) \le E_{B,i}^{\max}, \\ |v_{B,i}(t)| \le P_{B,i}^{\max} \end{cases} \tag{6}$$

Given the predefined time step $\Delta t \ll 1$ for (short-time scale) secondary level control, the output power $v_{B,i}(t)$ can be approximated with

$$v_{B,i}(t) = \frac{x_{B,i}(t) - x_{B,i}(t - \Delta t)}{\Delta t} \tag{7}$$

where $x_{B,i}(t - \Delta t) = \xi_{B,i}$ denotes the energy storage of the ith BESS at the previous time step which is assumed to be known at the current step; this is a reasonable assumption given the 'smart' cyber-physical nature of the MG.

By applying (7), the constraints are shown in (6) can be represented as

$$\max\{0, \xi_{B,i} - \Delta t P_{B,i}^{\max}\} \le x_{B,i}(t) \le \min\{E_{B,i}^{\max}, \xi_{B,i} + \Delta t P_{B,i}^{\max}\} \tag{8}$$

Considering the limited energy capacity of each BESS during power balance, the objective of each BESS is to maximise the stored energy, which is modelled as

$$\max \; x_{B,i}(t) \tag{9}$$

The authors would like to emphasise that if the BESS is fully charged and desired to implement power absorption, additional action can be implemented to reduce the stored energy by supporting external loads.

DDG unit: In the proposed framework, the dynamics of DDG unit i is described by the dynamics of its actual output power, which is modelled as follows:

$$P_{G,i}(s) = G_{G,i}(s) P_{G,i}^{*}(s) \tag{10}$$

where $P_{G,i}(s)$ is the output power of DDG unit i, $P_{G,i}^{*}(s) = u_{G,i}(s)$ is the set point for the output power of DDG unit i and is also the control signal in the proposed framework, $G_{G,i}(s)$ denotes the transfer function of DDG unit i and is defined as follows:

$$G_{G,i}(s) = \frac{k_{G,i}}{a_{G,i} s^2 + b_{G,i} s + 1} \tag{11}$$

where $k_{G,i}$, $a_{G,i}$, and $b_{G,i}$ are parameters that characterise the dynamics of the ith DDG unit by considering the time scale of the proposed control strategy.

Based on (10), letting $x_{G,i}(t) = P_{G,i}(t)$ and $v_{G,i}(t) = \mathrm{d}x_{G,i}(t)/\mathrm{d}t$ be the set point adjustment, the state-space equations of DDG unit i are achieved as follows:

$$\begin{cases} \dot{x}_{G,i}(t) = v_{G,i}(t), \\ \dot{v}_{G,i}(t) = -\dfrac{b_{G,i}}{a_{G,i}} v_{G,i}(t) - \dfrac{1}{a_{G,i}} x_{G,i}(t) + \dfrac{k_{G,i}}{a_{G,i}} u_{G,i}(t) \end{cases} \tag{12}$$

Because each DDG unit i can only inject power up to a maximum value $V_{\max,i}^{G}$ for set point adjustment of output power, a state constraint is obtained as

$$\begin{cases} x_{G,i}(t) \ge 0, \\ |v_{G,i}(t)| \le V_{\max,i}^{G} \end{cases} \tag{13}$$

Since $\Delta t \ll 1$ for (short-time scale) secondary level control, $v_{G,i}(t)$ can be approximated as follows:

$$v_{G,i}(t) = \frac{x_{G,i}(t) - x_{G,i}(t - \Delta t)}{\Delta t} \tag{14}$$

where $x_{G,i}(t - \Delta t) = \xi_{G,i}$ is known. Using (14), the constraints can be represented as shown in (13) as follows:

$$\max\left\{0, \xi_{G,i} - V_{\max,i}^{G} \Delta t\right\} \le x_{G,i}(t) \le \xi_{G,i} + V_{\max,i}^{G} \Delta t \tag{15}$$

CL unit: The dynamics of Load i are described as follows:

$$P_{L,i}(s) = G_{L,i}(s) P_{L,i}^{*}(s) \tag{16}$$

where $P_{L,i}(s)$ is the power demand of Load i, $P_{L,i}^{*}(s) = u_{G,i}(s)$ is the set point for the power demand of Load i and is also the control signal in the proposed framework, $G_{L,i}(s)$ denotes the transfer function of Load unit i and is defined as follows:

$$G_{L,i}(s) = \frac{k_{L,i}}{a_{L,i} s^2 + b_{L,i} s + 1} \tag{17}$$

where $k_{L,i}$, $a_{L,i}$, and $b_{L,i}$ are parameters that characterise the dynamics of the ith CL units by considering the time scale of the proposed control strategy. Based on (16), letting $x_{G,i}(t) = P_{G,i}(t)$ and $v_{G,i}(t) = \mathrm{d}x_{G,i}(t)/\mathrm{d}t$ be the set point adjustment, it can be achieved

$$\begin{cases} \dot{x}_{L,i}(t) = v_{L,i}(t), \\ \dot{v}_{L,i}(t) = -\dfrac{b_{L,i}}{a_{L,i}} v_{L,i}(t) - \dfrac{1}{a_{L,i}} x_{L,i}(t) + \dfrac{k_{L,i}}{a_{L,i}} u_{L,i}(t) \end{cases} \tag{18}$$

Given that each Load i can only consume power from the grid and the power consumption cannot exceed the power generation from the DDGs and BESSs, we can obtain the following constraint:

$$x_{L,i}(t) \le 0 \tag{19}$$

By considering the different priorities of critical and noncritical load units as well as the need to effectively service customers, the objectives of loads can be modelled as follows:

$$\begin{cases} \min \left| \sum_{i=1}^{n} w_{L,i} x_{L,i} - P_D \right|, \\ \min \sum_{i=1}^{n} w_{L,i} |x_{L,i} - \xi_{L,i}| \end{cases} \tag{20}$$

where $0 \le w_{L,i} \le 1$ is the positive weight representing the priority of Load i and satisfying $\sum_{i=1}^{n} w_{L,i} = 1$. The load with larger weight has higher priority. $\xi_{L,i}$ is the power demand of Load i at the previous time step that is available, and P_D is the desired weighted total power demand. The first optimisation in (10) aims to ensure the overall power demand of the system, and the second optimisation addresses the needs of minimising the change of the load consumption between the consistent time steps.

3.2.2 Components' interaction: The following objective needs to be met in order to achieve the power balance in the MG:

$$\min_{x_{G,i}(t),\, x_{L,i}(t)} \left| \sum_{i=1}^{k} [v_{B,i}(t) + P_{S,i}] + \sum_{i=1}^{m} x_{G,i}(t) + \sum_{i=1}^{n} x_{L,i}(t) \right| \tag{21}$$

where $P_{S,i}$ is the sum of the total power output of the *uncontrollable* units that are associated with BESS i. The audience should note that (21) expresses the need for power balance within the MG where the net power from BESSs ($\sum_{i=1}^{k} v_{B,i}(t)$) and DDGs ($\sum_{i=1}^{m} x_{G,i}(t)$) remaining after CLs are served ($\sum_{i=1}^{n} x_{L,i}(t)$) must compensate for the power deficit between uncontrollable loads and RESs (P_S). By substituting (7) into (21), we can get the following equation:

$$\min \left| \frac{1}{\Delta t} \sum_{i=1}^{k} x_{B,i}(t) + \sum_{i=1}^{m} x_{G,i}(t) + \sum_{i=1}^{n} x_{L,i}(t) - \frac{\xi_B}{\Delta t} + P_S \right| \tag{22}$$

where $P_S = \sum_{i=1}^{k} P_{S,i}$.

3.2.3 Model control strategy: The control signal $\boldsymbol{u}(t)$ is designed to achieve the objective functions (9), (20), and (22) with the constraints (6), (13), and (19). The objectives and associated constraints are described as follows:

$$\begin{cases} \max \ x_{B,i}(t), \\ \min \left| \sum_{i=1}^{n} x_{L,i} - P_D \right|, (w_{L,i} = 1), \\ \min \left| \frac{1}{\Delta t} x_B(t) + \sum_{i=1}^{m} x_{G,i}(t) + \sum_{i=1}^{n} x_{L,i}(t) - \frac{\xi_B}{\Delta t} + P_S \right| \\ \text{s.t.} \begin{cases} 0 \le x_{B,i}(t) \le E_{B,i}^{\max}, \\ 0 \le x_{G,i}(t), \\ x_{L,i}(t) \le 0 \end{cases} \end{cases} \tag{23}$$

To simplify the representation, we adopt the matrix–vector notations as follows:

$$\begin{cases} \boldsymbol{x}(t) = [x_B(t), x_{G,1}(t), \ldots, x_{G,n}(t), x_{L,1}(t), \ldots, x_{L,n}(t)]^{\mathrm{T}}, \\ \boldsymbol{v}(t) = [v_B(t), v_{G,1}(t), \ldots, v_{G,n}(t), v_{L,1}(t), \ldots, v_{L,n}(t)]^{\mathrm{T}} \end{cases}$$

Rewriting (5), (12), and (18), with the above notations the following equations are obtained:

$$\begin{cases} \dot{\boldsymbol{x}}(t) = \boldsymbol{M}\boldsymbol{v}(t), \\ \dot{\boldsymbol{v}}(t) = \boldsymbol{A}\boldsymbol{v}(t) + \boldsymbol{B}\boldsymbol{x}(t) + \boldsymbol{C}\boldsymbol{u}(t) \end{cases} \tag{24}$$

where (see equation below). By assigning

$$\tilde{\boldsymbol{u}}(t) = \boldsymbol{A}\boldsymbol{v}(t) + \boldsymbol{B}\boldsymbol{x}(t) + \boldsymbol{C}\boldsymbol{u}(t) \tag{25}$$

It is able to rewrite (24) as

$$\begin{cases} \dot{\boldsymbol{x}}(t) = \boldsymbol{v}, \\ \dot{\boldsymbol{v}}(t) = \tilde{\boldsymbol{u}}(t) \end{cases} \tag{26}$$

Based on (2), the potential function is designed as follows:

$$\begin{aligned} \Phi(t) = {} & \alpha_1 \left(\boldsymbol{w}_1^T \boldsymbol{x}(t) - P_D \right)^2 + \alpha_2 \left(\boldsymbol{w}_2^T \boldsymbol{x}(t) - \frac{\xi_B}{\Delta t} + P_S \right)^2 \\ & + \alpha_3 \sum_{i=1}^{k} \left(\boldsymbol{w}_3^T \boldsymbol{x}(t) - E_{B,i}^{\max} \right)^2 \end{aligned} \tag{27}$$

where $\boldsymbol{w}_1$ is a column vector whose elements are defined as follows:

$$\boldsymbol{w}_1(i) = \begin{cases} 0, & \text{if } i \le (m+k), \\ 1, & \text{otherwise} \end{cases} \tag{28}$$

$\boldsymbol{w}_2$ is a column vector whose elements are defined as follows:

$$\boldsymbol{w}_2(i) = \begin{cases} \frac{1}{\Delta t}, & \text{if } i \le k, \\ 1, & \text{otherwise} \end{cases} \tag{29}$$

$\boldsymbol{w}_3$ is a column vector whose elements are defined as follows:

$$\boldsymbol{w}_3(j) = \begin{cases} 1, & \text{if } i = j, \\ 0, & \text{otherwise} \end{cases} \tag{30}$$

The system-level stability is achieved when the output power of BESS converges to 0, the output power of DDGs is stable and the power demand of dynamic loads is stable. This is modelled by designing the control signal to achieve the following requirements:

$$\boldsymbol{v}(t) \to 0 \tag{31}$$

Letting the Laplacian matrix $\boldsymbol{L}$ represent the communication between BESS, DDGs and dynamic loads, whose elements are defined as follows:

$$\boldsymbol{L}(i,j) = \begin{cases} 1, & \text{if } i = j; \\ -\frac{1}{k+m+n}, & \text{otherwise} \end{cases} \tag{32}$$

The control signal $\tilde{\boldsymbol{u}}(t)$ is designed as follows:

$$\tilde{\boldsymbol{u}}(t) = -\bigtriangledown \Phi(t) - \boldsymbol{L}\boldsymbol{v}(t) - \beta(\boldsymbol{v}(t) - 0) \tag{33}$$

where β is a positive parameter. Based on (25), $\boldsymbol{u}(t)$ can be designed as follows:

$$\boldsymbol{C}\boldsymbol{u}(t) = -\bigtriangledown \Phi(t) - \boldsymbol{B}\boldsymbol{x}(t) - (\boldsymbol{L} + \boldsymbol{A} + \beta \boldsymbol{I})\boldsymbol{v}(t) \tag{34}$$

where $\boldsymbol{I}$ is a $(k+m+n)$-dimensional identity matrix. Letting $\Psi(t) = \bigtriangledown \Phi(t)$, its ith element ψ_i can be calculated using (27) as follows:

$$\psi_i = \begin{cases} \boldsymbol{h}_1^T \boldsymbol{x} - \frac{2\alpha_2 \xi_B}{(\Delta t)^2} + \frac{2\alpha_2 P_S}{\Delta t} - 2\alpha_3 E_{B,\max}, & \text{if } i \le k, \\ \boldsymbol{h}_2^T \boldsymbol{x} - \frac{2\alpha_2 \xi_B}{\Delta t} + 2\alpha_2 P_S, & \text{if } (k+1) \le i \le (m+k), \\ \boldsymbol{h}_3^T \boldsymbol{x} - 2\alpha_1 P_D - \frac{2\alpha_2 \xi_B}{\Delta t} + 2\alpha_2 P_S, & \text{otherwise} \end{cases} \tag{35}$$

$$\begin{cases} M = \mathrm{diag}(-1, \ldots, -k, 1 \ldots, 1) \\ A = \mathrm{daig}\left(-\frac{b_{B,1}}{a_{B,1}}, \ldots, -\frac{b_{B,k}}{a_{B,k}}, -\frac{b_{G,1}}{a_{G,1}}, \ldots, -\frac{b_{G,m}}{a_{G,m}}, -\frac{b_{L,1}}{a_{L,1}}, \ldots, -\frac{b_{L,n}}{a_{L,n}} \right) \\ B = \mathrm{daig}\left(-\frac{1}{a_{B,1}}, \ldots, -\frac{1}{a_{B,k}}, -\frac{1}{a_{G,1}}, \ldots, -\frac{1}{a_{G,m}}, -\frac{1}{a_{L,1}}, \ldots, -\frac{1}{a_{L,n}} \right) \\ C = \mathrm{daig}\left(-\frac{k_{B,1}}{a_{B,1}}, \ldots, -\frac{k_{B,k}}{a_{B,k}}, -\frac{k_{G,1}}{a_{G,1}}, \ldots, -\frac{k_{G,m}}{a_{G,m}}, \frac{k_{L,1}}{a_{L,1}}, \ldots, \frac{k_{L,n}}{a_{L,n}} \right) \end{cases}$$

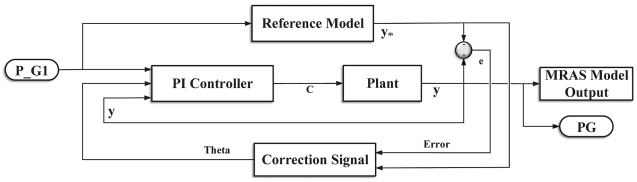

Fig. 2 *Model reference adaptive control system structure*

where α_l with $l = 1, 2, 3$ is positive parameter introduced in (27), Δt is time step, P_D is the total desired load demand for the MG, $E_{B,\max}$ is the maximum energy output of BESS, ξ_B is the energy output of BESS at a previous time step, $\boldsymbol{h}_1 = (2\alpha_2/\Delta t)\boldsymbol{w}_2 + 2\alpha_3\boldsymbol{w}_3$, $\boldsymbol{h}_2 = 2\alpha_2\boldsymbol{w}_2$, and $\boldsymbol{h}_3 = 2\alpha_1\boldsymbol{w}_1 + 2\alpha_2\boldsymbol{w}_2$, and the ith component of $\boldsymbol{h}_l$ with $l = 1, 2, 3$, can be represented as follows, respectively:

$$\boldsymbol{h}_1(i) = \begin{cases} \dfrac{2\alpha_2}{(\Delta t)^2} + 2\alpha_3, & \text{if } i \le k, \\ \dfrac{2\alpha_2}{\Delta t}, & \text{otherwise} \end{cases}$$

$$\boldsymbol{h}_2(i) = \begin{cases} \dfrac{2\alpha_2}{\Delta t}, & \text{if } i \le k, \\ 2\alpha_2, & \text{otherwise} \end{cases}$$

$$\boldsymbol{h}_3(i) = \begin{cases} \dfrac{2\alpha_2}{\Delta t}, & \text{if } i \le k, \\ 2\alpha_2, & \text{if } (k+1) \le i \le (m+k), \\ 2\alpha_1 + 2\alpha_2, & \text{otherwise} \end{cases}$$

Since the matrices $\boldsymbol{A}$, $\boldsymbol{B}$, and $\boldsymbol{C}$ are all diagonal matrices, a_i, b_i, and c_i are used to represent their ith diagonal element, respectively. Therefore, the control signal for the ith component of the MG $u_i(t)$ can be calculated as follows:

$$u_i(t) = -\frac{1}{c_i}\left[\psi_i + b_i x_i(t) + (1 + a_i + \beta)v_i(t) - \frac{1}{m+n}\sum_{j \ne i} v_j(t)\right] \tag{36}$$

where β is the positive parameter introduced in (33) and

$$a_i = \begin{cases} -\dfrac{b_{B,i}}{a_{B,i}}, & \text{if } i \le k, \\ -\dfrac{b_{G,i}}{a_{G,i}}, & \text{if } (k+1) \le i \le (m+k), \\ -\dfrac{b_{L,i}}{a_{L,i}}, & \text{otherwise} \end{cases}$$

$$b_i = \begin{cases} -\dfrac{1}{a_{B,i}}, & \text{if } i \le k, \\ -\dfrac{1}{a_{G,i}}, & \text{if } (k+1) \le i \le (m+k), \\ -\dfrac{1}{a_{L,i}}, & \text{otherwise} \end{cases}$$

$$c_i = \begin{cases} -\dfrac{k_{B,i}}{a_{B,i}}, & \text{if } i \le k, \\ -\dfrac{k_{G,i}}{a_{G,i}}, & \text{if } (k+1) \le i \le (m+k), \\ -\dfrac{k_{L,i}}{a_{L,i}}, & \text{otherwise} \end{cases}$$

3.2.4 Velocity matching based on MRAS: In order to achieve velocity matching and to optimise the performance of the system, we incorporated an MRAS [29] for the MG secondary control. We use two models for two sets of signals of generation including ESS, and demand to minimise the effects of interaction between the load and generation controlling efforts. The total weighted load and generation matrices are subject to a recursive procedure of error minimisation against a reference ideal plant where the outputs of the total load and generation systems are measured against the optimal model with the parameters of a_g^*, b_g^*, and k_g^* for the generation model, as follows:

$$\boldsymbol{G}^*(s) = \frac{k_g^*}{a_g^* s^2 + b_g^* s + 1} \tag{37}$$

$$\boldsymbol{y}_m = P_{G_1} G^* \tag{38}$$

where y_m is the output of our reference model. Now, we need to introduce our designated MIT (Massachusetts Institute of Technology) rule; MIT rule was first, developed by the MIT during the 1960s and is widely used to define the relationship between the changes of θ and the controlling signal [30] in adaptive control algorithms. The estimated and normalised sensitivity parameters from the MIT rule are exploited to achieve the parameters of the closed-loop control model meaning that the resulting model output error measured in the real plant is then fed to a first-order, regulator with the output modification signal of θ that is in turn fed to a simple proportional, integral, derivative (PID) controller [31] per the following:

$$\frac{\partial \boldsymbol{\theta}}{\partial \boldsymbol{t}} = \gamma e \tag{39}$$

where γ is the correction ratio (usually set as ≤ 0.01) and e is the model error

$$\boldsymbol{e} = y - y_m \tag{40}$$

where y is the real model output. The controlling model is presented in Fig. 2. The PID controller parameters are derived to maximise the speed and the rate of reference following in the model and minimise the output volatilities. The controlling signal can be written as a combination of the total generation, correction factor θ, and the plant's output as shown in the following equations:

$$\boldsymbol{c} = \theta u_c \tag{41}$$

$$\boldsymbol{u}_c = (P_{G_1} - y)\left(P_K + \frac{P_I}{s} + P_D s\right) \tag{42}$$

where P_K, P_I, and P_D are, respectively, proportional, integral, and differential coefficients of the PID controller presented in Fig. 2 whose values are fine-tuned to maximise the performance and speed of the adaptive system. In most cases P_D is assumed to be zero to reduce inaccuracy especially versus sinusoidal signals. The plant is the model of the system described in (10)–(12). The model for the load units is described as follows:

$$L^*(s) = \frac{k_l^*}{a_l^* s^2 + b_l^* s + 1} \tag{43}$$

where a_l^*, b_l^*, and k_l^* are the parameters illustrated in Fig. 2. These parameters are applied to the load units rather than generation units. The set points for the real model are acquired from the

Table 2 Parameters of MG units

Unit	Type	Power, KW	Peak/nominal
PV panels	generation	40	peak/combined
WT	generation	30	peak/combined
diesel generator	generation	180	nominal
sync. generator	generation	120	nominal
load 1	demand	800	peak
load 1	demand	240	nominal
load 2	demand	800	peak
load 2	demand	180	nominal
BESS	both	280	peak

flocking algorithm model regarding the CL. Furthermore, the adaptive algorithm based on the reference model is designed to facilitate managing and controlling the total load and generation, containing both controllable and uncontrollable units.

4 MG model

Given the high penetration of distributed generation in MG systems, inverters (that convert direct current to alternating current or vice versa) dominate the network. It is well known that effective control strategies for inverters are crucial for MG operation especially during autonomous operation. There are two common approaches to inverter control [32]. In the first approach, PQ inverter control uses the inverter to supply a given active and reactive power set-point. In the second approach, VSI [33] control uses the inverter to feed the load with pre-defined values for voltage and frequency facilitating power sharing amongst distributed generators [34]. The distributed generation in the proposed MG model operates with PQ control and corresponds to controllable units. Distributed generation operating with VSI control is taken into account in the objective function by P_s in (22). Since the capacity in terms of power and energy are limited for VSI controlled components, the goal is to distribute the required power required by adjusting PQ controlled components. Based on the power output measurement of VSI-controlled distributed generators, PQ-controlled distributed generators change their variables to ensure the entire power balance is achieved. Thus, the proposed control strategy is implemented to set appropriate reference power through secondary power adaptive control.

The test system consists of a synchronised generator, a PV unit, a BESS, a gas turbine, a WT, a diesel generator, and two loads. The parameters of the MG components are presented in Table 2. In our simulations, our proposed control strategy is implemented to control the synchronised generator, BESS, PV unit, diesel generator, and CL. The uncontrollable units, such as WT and gas turbine, only inform the BESS of their power output via one-directional communication. The BESS, diesel generator, and CL are modelled by using the dynamics of ESS, DDG, and CL units described in (5), (14), and (22), respectively.

The flocking control algorithm is embedded within the control centre of the test system presented in Fig. 3. The measurements on the total power generation and demand are fed into the flocking-based control mechanism whose Simulink model is provided in the Appendix. After being sampled and truncated, the measurements are used to implement (27) to achieve $\Phi(t)$ that is used to calculate the control signals via (36) for the synchronised generator, BESS, PV unit, diesel generator, and the loads, respectively. The parameters used in the reference models are specified in Table 3. The measurement-driven method, with a second-order model, has also been shown to effectively characterise the power with voltage as input [28].

5 Simulations and performance assessment

Various contingencies occurring during the operation can result in the instability of MGs. In our simulation, we consider three scenarios associated with three different categories of contingency: failure in the system generation apparatus, sudden and unexpected demand surges in the MGs demand models, and system control model being compromised due to external activities. In each of these three scenarios, we evaluate the resilience of the proposed control method against the considered undesired condition. So three different scenarios for the emergency operation of the MG of Fig. 3 are investigated to evaluate the performance of our proposed flocking-based adaptive granular control. The proposed flocking-based control mechanism is implemented throughout the simulation to demonstrate its capabilities to be resilient to severe disturbances. In each scenario, we evaluate the performance of our control strategy in face of the various disturbances that occur during the damping period and steady-state period. The performance of the system under singular disturbances is also evaluated to enable a comparison between the response of the system to different situations and evaluate the extent of capabilities of the system. Due to the high computation level of the system, we use a real-time simulator, OPAL-RT Technologies^{TM} *OP5600*, to simulate our testbed shown in Fig. 3. It also enabled real-time adjustments of the disturbances to the system and evaluate their effects simultaneously.

5.1 Distributed generator contingency

Generator contingency in the MGs has the impact of interrupting active power supply, and thus its restoration (via leveraging other resources) is crucial for the MG survival. The proposed algorithm is effective to enforce cooperation amongst controllable units so that when there is insufficient or lost power from one generator, the other units will be forced through the adaptive algorithm to stabilise the system and compensate the loss of generation. In Fig. 4, we show a simulation result for comparing the performance of the proposed flocking-based adaptive method with the PID control that is a well-established method. As shown in Fig. 4, we can observe that the proposed flocking-based adaptive method can achieve power balance faster. This is due to the fact that normal control approaches do not utilise the fast response of ESSs while our proposed adaptive approach effectively exploits the cooperation between energy storage and other MG units. Furthermore, the response of the additional generation units under flocking-based adaptive model is considerably faster than that of a PID controller. In the first case study, diesel generator suffers a significant loss of generation at $t = 20$ s to model the impact of a disturbance. The active power outputs from the other controllable units are presented in Fig. 5, from which it can be observed that at the time $t = 20$ s, the contingency on the diesel generator results in the battery energy storage to immediately participate in generating power for the MG. At the same time, another generator and DG unit increase their generation significantly to compensate this loss as it can be seen in Fig. 5*a*. The BESS and PV panels generation levels gradually stabilise and go back into its normal operation, and each CL achieves its desired power demand. Fig. 5*b* shows that stability is achieved in $t = 50$ s. Therefore, by intelligently determining the set points of the controllable MG components, the proposed control strategy effectively maintains the system-level stability of the MG in the presence of the contingency on distributed generators. Fig. 5*b* also illustrates the performance of the proposed granular flocking-adaptive controller in controlling various portions of the MG's performance. We also link the responses of generators to certain events in the system where certain contingency scenarios, trigger certain generation for example demand surge would activate a certain source unit while the loss in generation regardless of the balance, would activate another. In Fig. 5*a*, two disturbances occur simultaneously, meaning that the loss in power generation in the diesel generator leads to a negative balance which activates multiple generation units as shown in the plots during the duration between $t = 20$ s and $t = 30$ s. In the second case, we evaluate the performance of our proposed control strategy by considering another scenario in which the generation loss and recovery in diesel generator occurs consecutively during the damping and steady-state period of the system as shown in Fig. 6. From Fig. 6, it is clear that in this scenario our controlling strategy is also effective in compensating the system generation loss and achieving the power balance and going back to resting phase after the system is recovered. We

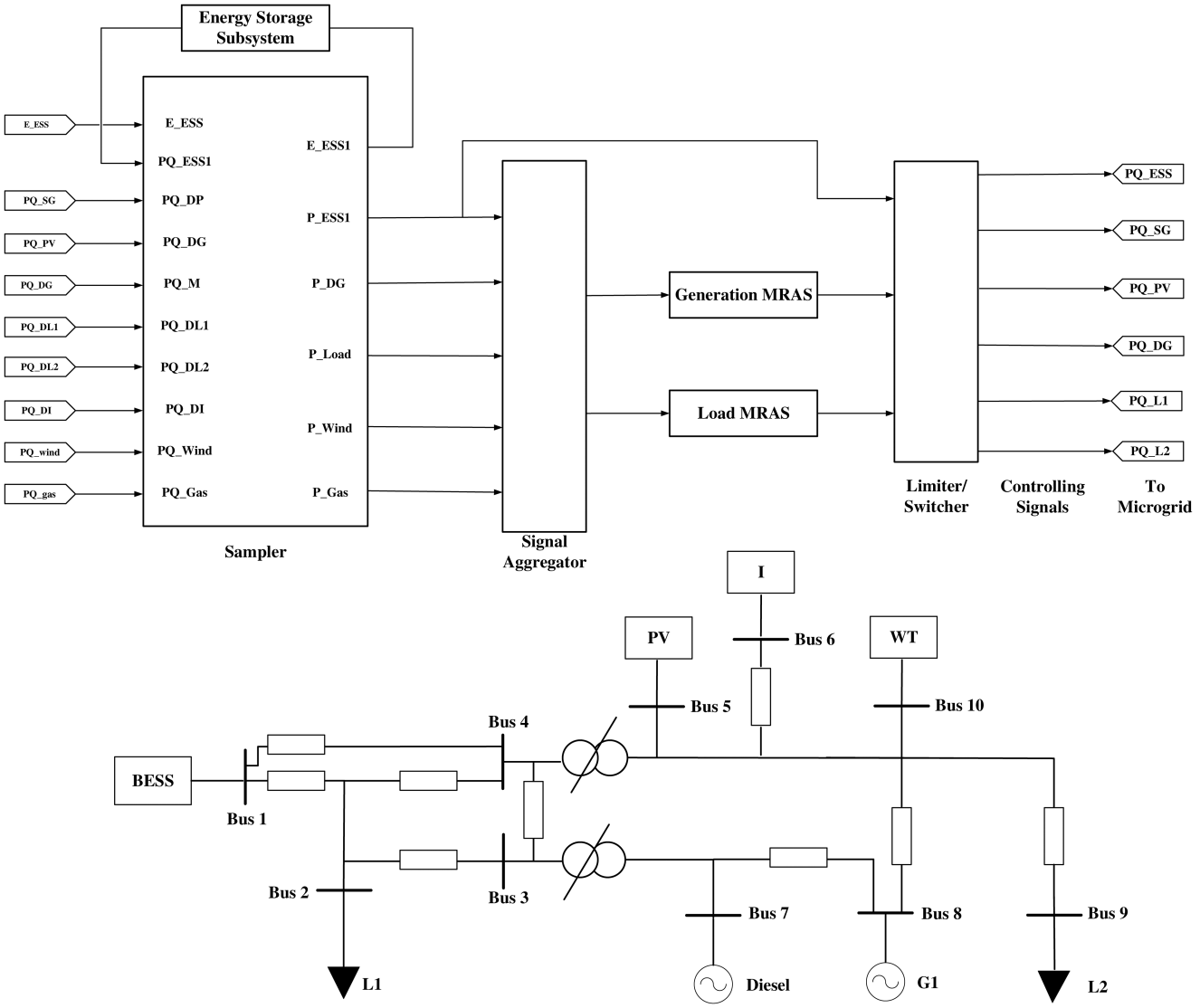

Fig. 3 *Test system of MG*

Table 3 Summary of control parameters

Parameter	Value
(a_g^*, b_g^*, k_g^*)	(1.5, 1.1, 1)
(a_l^*, b_l^*, k_l^*)	(2, 8, 1)
α_1	1
α_2	0.5
α_3	0.1
β	1

would like to mention that a 5 kW cushion is designed to remain in the generation system which is used to charge the BESS. Additional simulation results are provided in the Appendix.

5.2 Demand surge

An MG can be subject to wide variations in load due to the unexpected changes in human demand and activities. Multiple appliances could be turned on at the same time by chance, resulting in a sudden increase in demand and leading to demand surge in certain nodes. To evaluate the resilience of our proposed method to this demand surge, in this scenario we consider a sudden increase in demand as well as the activation of the second load. The simulation results demonstrate how the flocking algorithm changes rapidly the generator set point to meet the power balance and the adaptive algorithm neutralises the volatilities form the load surge. It is assumed that, from time $t = 25$ s, the CL L1 increases its power demand by 50 kW. In the meantime, G1 gradually increases the power generation to take an equal share of the increased power demand. The power balance is achieved after $t = 35$ s as shown in Fig. 7, from which it can be seen that the proposed control strategy can efficiently maintain the system-level stability of MG in the face of an unexpected increase in demand as well as non-linearity in the demand.

In this case study, we first consider the demand increase of different levels occurring during the steady-state period of the system and evaluate the effectiveness of our proposed control strategy in achieving power balance in these individual cases, which is shown in Fig. 8.

In addition, we consider another scenario in which there are consecutive demand increases occurring within a short-time duration. In this scenario, one sudden demand increase of 50 kW occurs on load L1 at $t = 40$ s and another demand increase of 50 kW occurs on load L2 at $t = 70$ s. The performance of the system is illustrated in Fig. 9. From Fig. 9, it is clear that our proposed control strategy is capable of effectively conquering the first demand increase but fails to handle the second disturbance, which results in the instability of the system. We believe this is because that the second disturbance occurs before the first one is fully addressed by our proposed control system.

Furthermore, to demonstrate the mechanism of our flocking-based control strategy in more details, we test the system with a set of combined disturbance signals, including a demand surge at $t = 35$ s and generation loss at $t = 70$ s. The individual units responses and balance load are presented, in Figs. 10*a* and *b*, respectively.

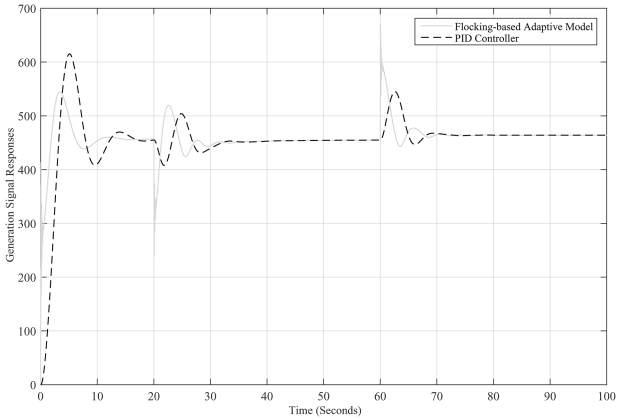

Fig. 4 *Generation response comparison in the MG under distributed generation loss*

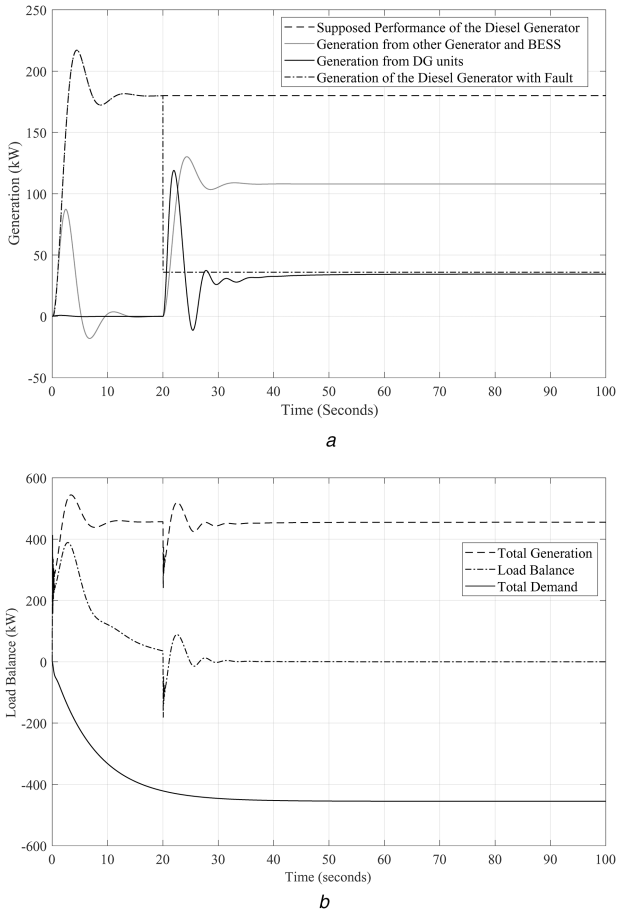

Fig. 5 *The active power for*
(a) Generation compensation in the microgrid units, ***(b)*** Cumulative generation, demand, and load balance

5.3 Cyber attack

Considering the high vulnerability of MGs to potential cyber attacks [15], in this case, a study we evaluate the performance of our proposed control mechanism in the presence of FDI attack that is one of the most critical cyber attacks to the power systems [20, 21, 35]. To achieve this goal, we simulate the FDI attacks by specifying the following threat model: (i) the attackers have some knowledge of the architecture of the MG and its control model, (ii) the attackers are capable to explore and modify some system measurements, and (iii) the attackers are able to compromise some controlling information such as set points. Furthermore, we consider that the FDI attacks are launched by altering the controlling information on the set points and by compromising the system measurements, respectively. We consider these two FDI attack strategies individually in the following subsections.

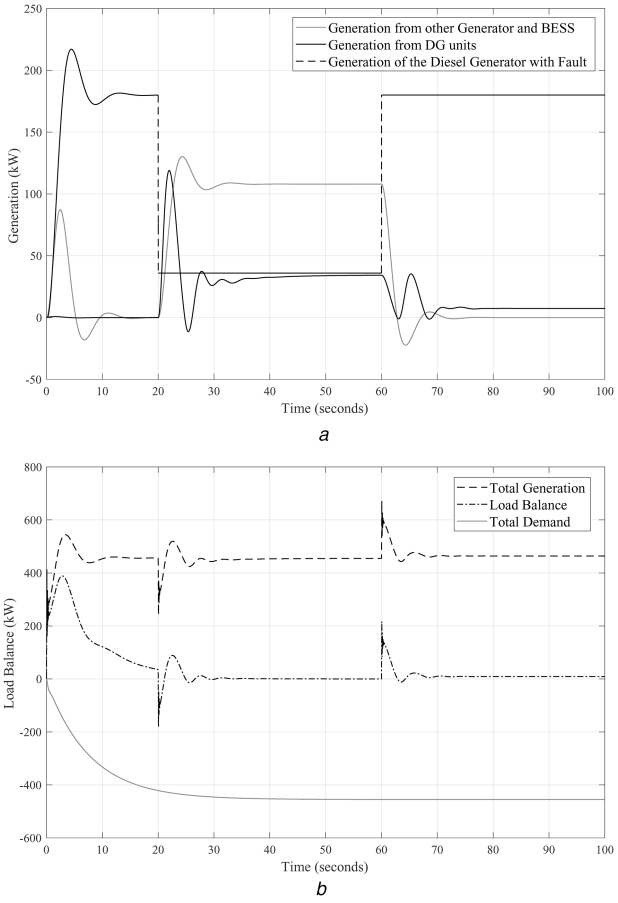

Fig. 6 *The active power in multiple scenarios*
(a) Generation compensation in a stable system, ***(b)*** Cumulative generation, demand, and load balance under consecutive loss and recovery

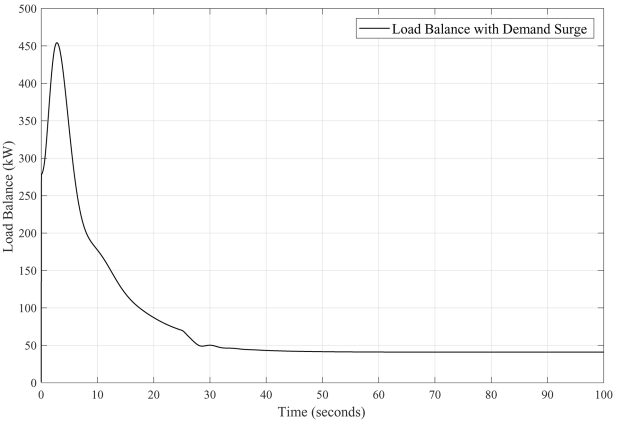

Fig. 7 *Power balance in face of demand surge*

5.3.1 Compromising controlling information: We assume that the attacker aims to hack the controlling information on the set points by either modifying the designated reference model or compromising the performance of the MRAS in the adaptive procedure. The performances of our control strategy, and compromised reference models, in face of similar disturbance under this FDI attack, are illustrated, respectively, in Fig. 11. As shown in Fig. 11, it is clear that the response of the compromised control controller suffers from very low damping rate as well as undamped harmonics that may lead to a negative balance in the long run. Also, the behaviour of the compromised model in its transient state, which can potentially endanger the functionality of the whole system, shows massive initial overshooting. Although the response of the reference model is greatly compromised, our granular flocking-based adaptive algorithm performance remains nearly identical and manages to fend off the effects of the FDIA within the model. This is due to the proper designated MIT rule

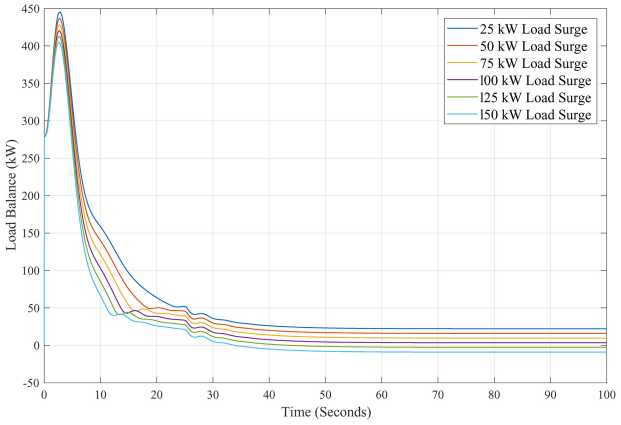

Fig. 8 *Effectiveness of our proposed control strategy when encountering the demand increase of 25, 50, 75, 100, 125, 150 kW*

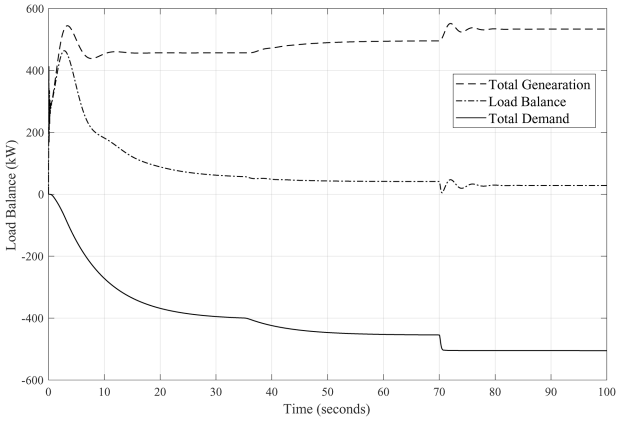

Fig. 9 *Power balance in the presence of multiple demand surges*

and flocking-based algorithm that enable the fast tracking and accurate response as well as the effective design of the adaptive adjustment portion of the MRAS controller.

5.3.2 Modifying system measurements: To evaluate the performance of our proposed control strategy, we consider a second scenario in which the attackers target at the parameters of the PID controller embedded within the MRAS blocks [31]. In this scenario, the parameters of the P_K, P_I, and P_D are modified to reduce the efficiency of the system. We compare the performance of the intact system with that of the system under attack in Fig. 12. From Fig. 12, it can be observed that our proposed control mechanism is effective in mitigating the FDI attack on the parameters of the PID controller, which are critical system measurements, and stabilising the system by applying MIT rule and flocking algorithm. Furthermore, it can be seen that, other than minimal excessive overshooting and undershooting, the system will demonstrate near identical performance due to effective adaptive system modelling. From the above three case studies, we can get that our proposed control strategy provides a reliable and quick-response secondary control for the islanded MG even in face of emergent generator contingency, unexpected demand surge at the cost of the all-to-all communication network.

6 Conclusions

In this paper, we propose a flocking-based granular adaptive control strategy for real-time power balance to enhance the system-level stability of autonomous MGs. The proposed biologically-inspired adaptive control strategy leverages the cooperation amongst the controllable units including ESSs, CLs, and generators and explores the capabilities of the system to facilitate resilience to disturbances, attacks, and surges in demand. This is carried out in three stages: modelling the dynamics of the MG, setting up a model-reference adaptive control system and finally facilitating

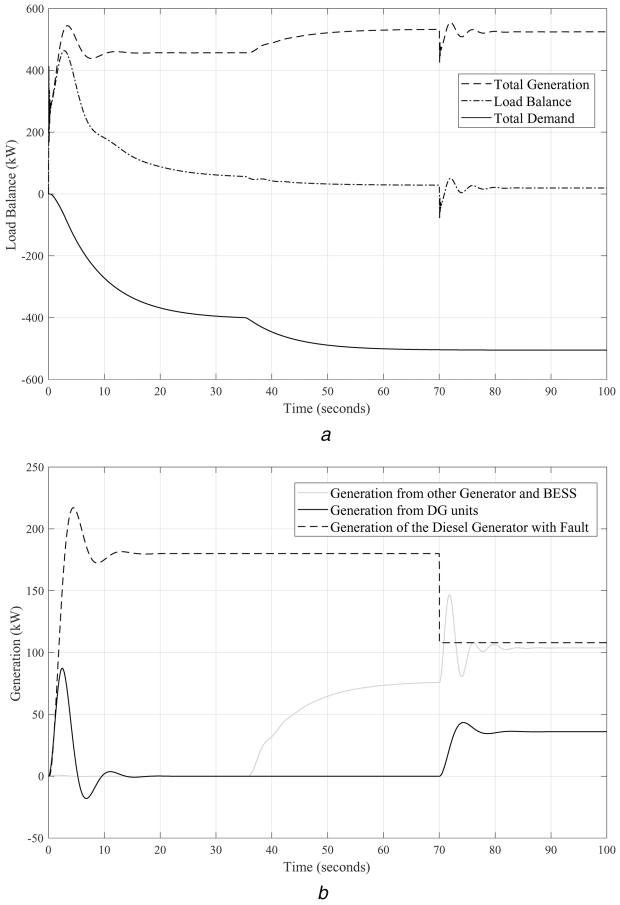

Fig. 10 *The active power for*
(a) Generation compensation in a stable system, ***(b)*** Load balance in presence of multiple disturbances within the microgrid units

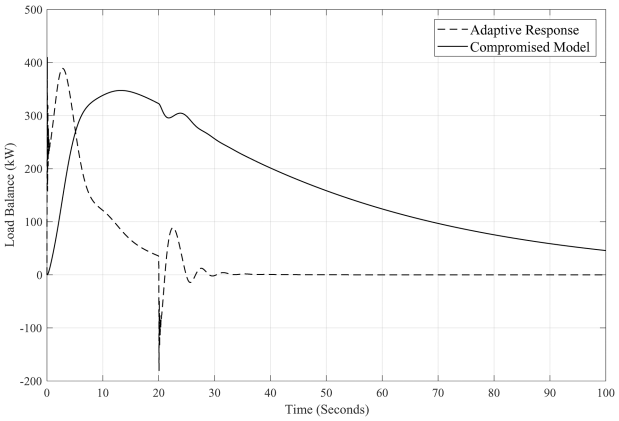

Fig. 11 *Comparison of the performance of the flocking-adaptive algorithm versus compromised reference response in face of FDI attacks on the reference model*

distributed ESSs to achieve power balance in the MG. As illustrated in the simulation results, our proposed control strategy is effective in achieving the power balance in the autonomous MGs in the presence of physical faults, demand surges, and cyber attacks. The authors assert that the proposed work will potentially promote the extensive deployment of resilient MGs that efficiently improve the quality of power supply from both technical and economical perspectives.

In the future, the authors will extend the current work in the following three directions: (i) moving towards an intelligent control paradigm by incorporating reinforcement learning algorithms, (ii) analysing the impact of the high penetration of renewable energy on the control strategy, and (iii) examining the resilience of the control strategy by considering more complex system topology.

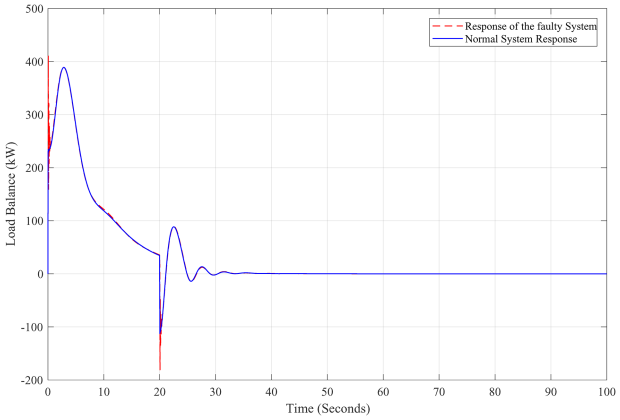

Fig. 12 *Response of the adaptive system with the altered controller versus normal performance*

7 References

[1] Gharavi, H., Hu, B.: 'Multigate communication network for smart grid', *Proc. IEEE*, 2011, **99**, pp. 1028–1045

[2] Wei, J., Kundur, D., Zourntos, T.: 'On the use of cyber-physical hierarchy for smart grid security and efficient control'. Proc. IEEE Canadian Conf. on Electrical and Computer Engineering (CCECE), Montreal, Canada, 2012

[3] Guerrero, J.M., Vasquez, J.C., Matas, J., *et al.*: 'Hierarchical control of droop-controlled ac and dc microgrids–A general approach toward standardization', *IEEE Trans. Ind. Electron.*, 2011, **58**, pp. 158–172

[4] Khodaei, A., Shahidehpour, M.: 'Microgrid-based co-optimization of generation and transmission planning in power systems', *IEEE Trans. Power Syst.*, 2013, **28**, pp. 1582–1590

[5] Mehrizi-Sani, A., Iravani, R.: 'Potential-function based control of a microgrid in islanded and grid-connected modes', *IEEE Trans. Power Syst.*, 2010, **25**, pp. 1883–1891

[6] Jaleeli, N., VanSlyck, L.S., Ewart, D.N., *et al.*: 'Understanding automatic generation control', *IEEE Trans. Power Syst.*, 1992, **7**, (3), pp. 1106–1122

[7] Lasseter, R., Akhil, A., Marnay, C., *et al.*: 'The certs microgrid concept, white paper on integration of distributed energy resources'. California Energy Commission, Office of Power Technologies-US Department of Energy, LBNL-50829, 2002. Available at http://certs lbl gov

[8] Katiraei, F., Iravani, R., Hatziargyriou, N., *et al.*: 'Microgrids management', *IEEE Power Energy Mag.*, 2008, **6**, (3), pp. 54–65

[9] Bidram, A., Lewis, F.L., Davoudi, A.: 'Distributed control systems for small-scale power networks: using multiagent cooperative control theory', *IEEE Control Syst.*, 2014, **34**, pp. 56–77

[10] Chen, Z., Luo, A., Wang, H., *et al.*: 'Adaptive sliding-mode voltage control for inverter operating in islanded mode in microgrid', *Int. J. Electr. Power Energy Syst.*, 2015, **66**, pp. 133–143

[11] Madureira, A., Moreira, C., Lopes, J.P.: 'Secondary load-frequency control for microgrids in islanded operation'. Proc. Int. Conf. on Renewable Energy and Power Quality (ICREPQ), Spain, 2005, pp. 1–5

[12] Lou, G., Gu, W., Wang, L., *et al.*: 'Decentralised secondary voltage and frequency control scheme for islanded microgrid based on adaptive state estimator', *IET Gener. Transm. Distrib.*, 2017, **11**, (15), pp. 3683–3693

[13] Xu, Y., Sun, H., Gu, W., *et al.*: 'Optimal distributed control for secondary frequency and voltage regulation in an islanded microgrid', *IEEE Trans. Ind. Inf.*, 2018, **PP**, (99), pp. 1–1

[14] Chen, C., Wang, J., Qiu, F., *et al.*: 'Resilient distribution system by microgrids formation after natural disasters', *IEEE Trans. Smart Grid*, 2016, **7**, (2), pp. 958–966

[15] Veitch, C.K., Henry, J.M., Richardson, B.T., *et al.*: 'Microgrid cyber security reference architecture'. Sandia ReportT, 2013

[16] Chlela, M., Mascarella, D., Joos, G., *et al.*: 'Fallback control for isochronous energy storage systems in autonomous microgrids under denial-of-service cyber-attacks', *IEEE Trans. Smart Grid*, 2017, **PP**, (99), pp. 1–1

[17] Farraj, A., Hammad, E., Kundur, D.: 'On the impact of cyber attacks on data integrity in storage-based transient stability control', *IEEE Trans. Ind. Inf.*, 2017, **13**, (6), pp. 3322–3333

[18] Rana, M.M., Li, L., Su, S.W.: 'Cyber attack protection and control of microgrids', *IEEE/CAA J. Autom. Sinica*, 2017, **PP**, (99), pp. 1–8

[19] Wang, Y., Amin, M.M., Fu, J., *et al.*: 'A novel data analytical approach for false data injection cyber-physical attack mitigation in smart grids', *IEEE. Access.*, 2017, **5**, pp. 26022–26033

[20] Basumallik, S., Eftekharnejad, S., Davis, N., *et al.*: 'Impact of false data injection attacks on PMU-based state estimation'. 2017 North American Power Symp. (NAPS), Morgantown, WV, USA, 2017, pp. 1–6

[21] He, Y., Mendis, G.J., Wei, J.: 'Real-time detection of false data injection attacks in smart grid: a deep learning-based intelligent mechanism', *IEEE Trans. Smart Grid*, 2017, **8**, (5), pp. 2505–2516

[22] Team, A.S.D.: 'Microgrid solutions for island utilities', 2017

[23] Zhang, W.L., Qiu, M., Lai, X.K.: 'Application of energy storage technologies in power grids', *Power Syst. Technol.*, 2008, **7**, pp. 3–9

[24] Reynolds, C.W.: 'Flocks, herds, and schools: a distributed behavioral model', *Comput. Graph.*, 1987, **21**, (4), pp. 25–34

[25] Olfati-Saber, R.: 'Flocking for multi-agent dynamic systems: algorithms and theory', *IEEE Trans. Autom. Control*, 2006, **51**, (3), pp. 401–420

[26] Feng, X., Butler-Purry, K.L., Zourntos, T.: 'A multi-agent system framework for real-time electric load management in MVAC all-electric ship power systems', *IEEE Trans. Power Syst.*, 2015, **30**, pp. 1327–1336

[27] Feng, X., Butler-Purry, K.L., Zourntos, T.: 'Multi-agent system-based real-time load management for all-electric ship power systems in dc zone level', *IEEE Trans. Power Syst.*, 2012, **27**, pp. 1719–1728

[28] Visconti, I., Lima, D., Costa, J., *et al.*: 'Measurement-based load modeling using transfer functions for dynamic simulations', *IEEE Trans. Power Syst.*, 2014, **29**, pp. 111–120

[29] Butler, H., van Amerongen, J., Honderd, G.: '*Model reference adaptive control: Bridging the gap between theory and practice*' (Universiteit Delft, Delft, Netherlands, 1990)

[30] Swarnkar, P., Jain, S., Nema, R.: 'Effect of adaptation gain on system performance for model reference adaptive control scheme using mit rule', *World. Acad. Sci. Eng. Technol.*, 2010, **70**, pp. 621–626

[31] Rivera, D.E., Morari, M., Skogestad, S.: 'Internal model control: Pid controller design', *Ind. Eng. Chem. Process Des. Dev.*, 1986, **25**, (1), pp. 252–265

[32] Lopes, J.P., Moreira, C., Madureira, A.: 'Defining control strategies for microgrids islanded operation', *IEEE Trans. Power Syst.*, 2006, **21**, (2), pp. 916–924

[33] Wang, F., Shen, W., Boroyevich, D., *et al.*: 'Voltage source inverter', *IEEE Ind. Appl. Mag.*, 2009, **15**, (2), pp. 24–33

[34] Moradian, M., Tabatabaei, F.M., Moradian, S.: 'Modeling, control & fault management of microgrids', *Smart Grid Renew. Energy*, 2013, **4**, (01), p. 99

[35] Liu, Y., Ning, P., Reiter, M.K.: 'False data injection attacks against state estimation in electric power grids', *ACM Trans. Inf. Syst. Secur. (TISSEC)*, 2011, **14**, (1), p. 13

8 Appendix

8.1 Extended simulation results

8.1.1 Frequency response: In this section, we provide the frequency responses for the system model. The frequency response in the cases considering singular and consecutive loss, respectively, is shown in Fig. 13 where it can be seen that the overall frequency response of the system at the distribution lines suffers slight variations. It is reasonable because of the fast response of the system. From Fig. 13, we can also observe the effective recovery effort that facilitates acceptable and fast recovery of the frequency at the end lines and prevents a significant surge in the frequency. Fig. 14 shows the frequency response in a scenario considering a consecutive demand surges. As shown in Fig. 14, there are two jumps in the frequency response, do not interrupt the stability of the system.

Furthermore, we also evaluate the performance of our method in the presence of cyber attacks. The cyber attack, we consider here is FDI attack. The frequency response of the system is presented in Fig. 15, from which we can observe the resilience of the proposed algorithm in mitigating the consequences of external disruption.

8.2 MG control mechanism illustration

As stated in Section 3, in our method the flocking-based mechanism is designed to sample, truncate and implement the allocated control tasks for generating control signals. The Simulink implementation of our flocking-based control mechanism is shown in Fig. 16.

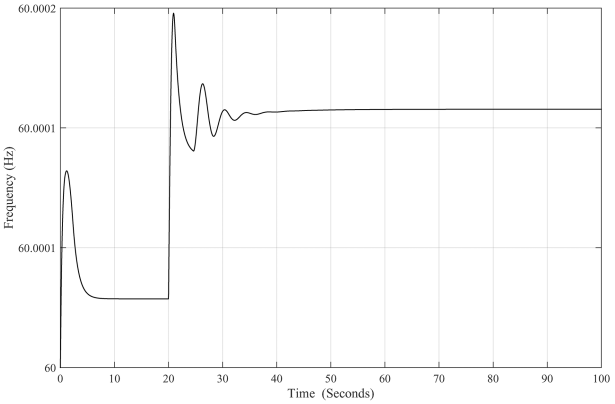

a

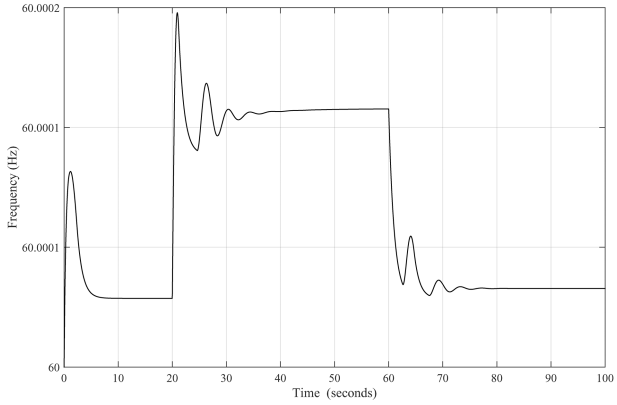

b

Fig. 13 *Frequency response under:*
(a) A single DG failure, ***(b)*** Consecutive loss and recovery in DG units

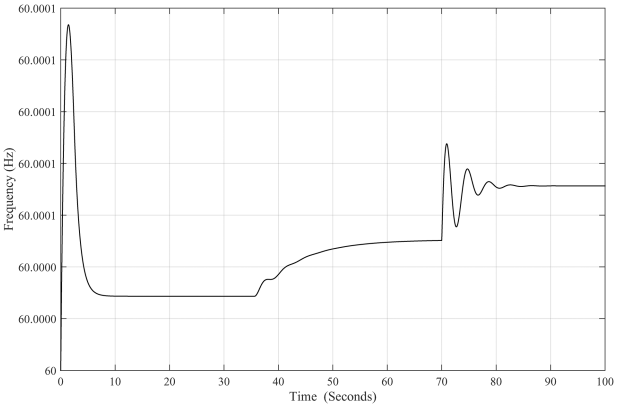

Fig. 14 *Frequency response under consecutive demand surges in the MG*

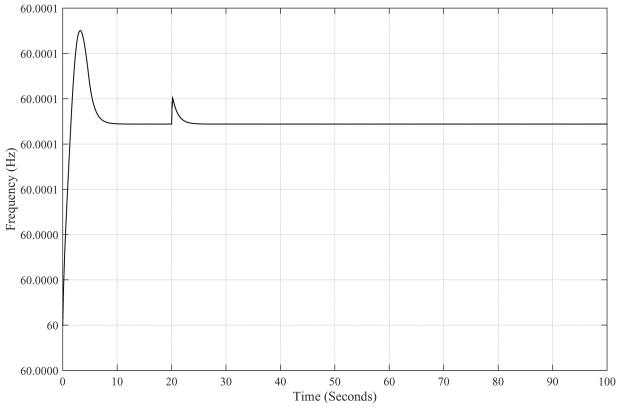

Fig. 15 *Frequency response in a system with a compromised control model*

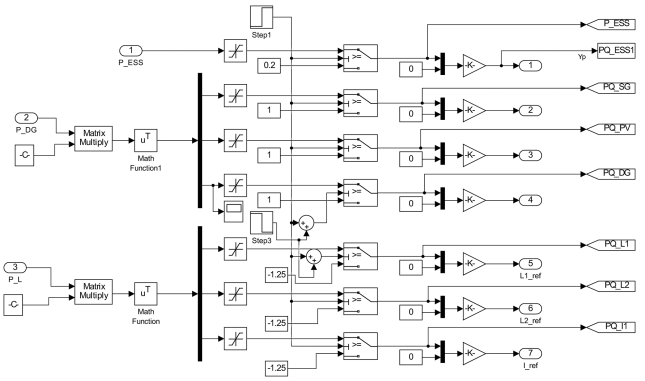

Fig. 16 *Simulation implementation of our flocking-based control mechanism*